The C57Bl/6 mouse serves as a suitable model of human skeletal muscle mitochondrial function

Robert A. Jacobs[1,2,4], Víctor Díaz[1,2,3], Anne-Kristine Meinild[1,4], Max Gassmann[1,2,5] and Carsten Lundby[1,4]

[1] *Zurich Center for Integrative Human Physiology (ZIHP) and*
[4] *Institute of Physiology, University of Zurich, Switzerland*
[2] *Institute of Veterinary Physiology, Vetsuisse Faculty, University of Zurich, Switzerland*
[3] *Department of Health and Human Performance, Universidad Politécnica de Madrid, Spain*
[5] *Universidad Peruana Cayetano Heredia (UPCH), Lima, Peru*

New Findings

- **What is the central question of this study?**
  Do mouse skeletal muscle mitochondria resemble human skeletal muscle mitochondria sufficiently to serve as a proper model and how do differences of skeletal muscle type affect the comparison?
- **What is the main finding and its importance?**
  We find that mouse skeletal muscle respiratory capacity and control function rather similar to human m. vastus lateralis, with the mouse quadricep being overall the most similar. This resemblance is not universal, however, because the coupling control of electron transport during fat oxidation in type I murine muscle is more comparable to human vastus lateralis.

It is debatable whether differences in mitochondrial function exist across skeletal muscle types and whether mouse skeletal muscle mitochondrial function can serve as a valid model for human skeletal muscle mitochondrial function. The aims of this study were to compare and contrast three different mouse skeletal muscles and to identify the mouse muscle that most closely resembles human skeletal muscle respiratory capacity and control. Mouse quadriceps ($QUAD_M$), soleus (SOL_M) and gastrocnemius ($GAST_M$) skeletal muscles were obtained from 8- to 10-week-old healthy mice ($n = 8$), representing mixed, oxidative and glycolytic muscle, respectively. Skeletal muscle samples were also collected from young, active, healthy human subjects ($n = 8$) from the vastis lateralis ($QUAD_H$). High-resolution respirometry was used to examine mitochondrial function in all skeletal muscle samples, and mitochondrial content was quantified with citrate synthase activity. Mass-specific respiration was higher across all respiratory states in SOL_M *versus* both $GAST_M$ and $QUAD_H$ ($P < 0.01$). When controlling for mitochondrial content, however, SOL_M respiration was lower than $GAST_M$ and $QUAD_H$ ($P < 0.05$ and $P < 0.01$, respectively). When comparing respiratory capacity between mouse and human muscle, $QUAD_M$ exhibited only one different respiratory state when compared with $QUAD_H$. These results demonstrate that qualitative differences in mitochondrial function exist between different mouse skeletal muscles types when respiratory capacity is normalized to mitochondrial content, and that skeletal muscle respiratory capacity in young, healthy $QUAD_M$ does correspond well with that of young, healthy $QUAD_H$.

Mouse modelling for the study of human health and disease is an extremely powerful tool that is widely used. The degree of conservation between mouse and human genomes permits the study of murine biology largely to characterize that of humans (Mouse Genome Sequencing Consortium *et al.* 2002). There remains, however, a biological divergence between species that is not always readily apparent and can lead to scientific misdirection if not properly recognized. There are certain fundamental differences in mouse models that mimic human disease with regard to cancer (Rangarajan & Weinberg, 2003), ageing (Demetrius, 2006) and metabolic disease (Svenson *et al.* 2007; Garland *et al.* 2011) that must be taken into account. The use of rodents for research on human muscle disuse and sarcopenia is fraught with dissimilarities between species (Rennie *et al.* 2010). The differences between mice and humans extend beyond diseased states. Haemodynamic control differs between healthy humans and mice (Desai *et al.* 1997; Bernstein, 2003), as do normal metabolic profiles of some skeletal muscles (Schiaffino *et al.* 2007). Accordingly, data extrapolation from mouse studies modelling human physiological function, in both healthy and diseased states, can have limitations if the differences between species are not identified and controlled for.

Mitochondria are associated with the aetiology of many disease states and disorders, including ageing (Jacobs, 2003) and metabolic disease (Lowell & Shulman, 2005; Chomentowski *et al.* 2011). The roles of mitochondrial function in these diseases are often studied using mouse models (Picard *et al.* 2010; Miller *et al.* 2012; Paglialunga *et al.* 2012; Sebastián *et al.* 2012). The most common tissue used to analyse mitochondria is skeletal muscle, because of its accessibility, relative mass-to-body weight ratio and high metabolic rate. Differences between mouse and human skeletal muscle have brought into question the validity of studying mouse mitochondria, and alternative animal models have already been proposed ostensibly to replace the mouse for the study of human mitochondrial physiology (Lemieux & Warren, 2012).

Skeletal muscle anatomy and function vary between mice and humans. These recognized differences have led to comparisons of molecular expression across different mouse and human muscles in an attempt to identify the best phenotypic association between species (Kho *et al.* 2006). The mouse soleus (SOL_M) has been reported to express the closest molecular resemblance to several human skeletal muscles (Kho *et al.* 2006). However, mitochondrial function across different murine skeletal muscles has never been empirically compared with a human skeletal muscle, namely the vastus lateralis, because that is the most common human skeletal muscle sampled. The aim of this study, therefore, is to analyse respiratory capacity and control across several mouse muscles and to evaluate those results with skeletal muscle mitochondrial function measured from young and healthy human subjects.

Our first objective is to compare and contrast mitochondrial function across the lateral portion of mouse quadriceps ($QUAD_M$), SOL_M and lateral gastrocnemius ($GAST_M$). Hitherto, differences in mitochondrial function across skeletal muscles have been attributed primarily to the differences in mitochondrial content (Hoppeler *et al.* 1987; Schwerzmann *et al.* 1989). Such studies, however, used preparations of isolated mitochondria for respirometric analysis with limited substrate supply, never reaching maximal state 3 respiration or oxidative phosphorylation capacity (P) of the entire respiratory system. We have previously demonstrated that differences in mitochondrial respiratory capacity and control are apparent only when substrate provision for both complex I (CI; NADH dehydrogenase) and complex II (CII; succinate dehydrogenase) is provided (Jacobs & Lundby, 2012). Our first objective is to confirm differences in respiratory capacity and control between different skeletal muscles as suggested by previous studies in humans (Amara *et al.* 2007; Conley *et al.* 2007). Our second objective is to determine whether mouse skeletal muscle can properly represent human skeletal muscle mitochondrial function and, if so, to identify the mouse skeletal muscle that best represents human muscle. Our hypotheses are as follows: (i) that the mouse can serve as a viable model for the study of mitochondrial function in humans; and (ii) that SOL_M will best represent mitochondrial function in human skeletal muscle, as a result of the molecular similarities between muscles (Kho *et al.* 2006).

Methods

Ethical approval

The experimental protocols using laboratory animals were approved by the Kantonales Veterinäramt Zürich (73/2011) and were performed in accordance with the Swiss animal protection laws and institutional guidelines. The Regional Ethics Committee of Region Hovedstaden in Denmark approved experimental protocols involving human subjects (H-1-2011-052), which were in accordance with the Declaration of Helsinki. Prior to the start of the experiments, informed oral and written consent was obtained from all participants.

Experimental animals

A total of eight C57Bl/6J wild-type mice were used in this study. All mice were housed in standard rodent cages with fixed temperature ($21 \pm 1^{\circ}C$), free access to food and water, and a 12 h–12 h light–dark cycle. Mice ranged from 8 to 10 weeks of age when they were killed and

skeletal muscles collected. Animals were killed by means of carbon dioxide inhalation, followed by rapid excision of $QUAD_M$, SOL_M and $GAST_M$. These muscles represent a mixed oxidative and glycolytic muscle, an oxidative muscle and a glycolytic muscle, respectively.

Human subjects

Eight young and physically active subjects voluntarily participated in this study. Subject characteristics (means ± SD) were as follows: age, 26 ± 5 years; height, 175 ± 9 cm; and body weight, 70 ± 7 kg. All subjects were recreationally active. No subjects were taking any sort of prescription medication or had any known family history of type 2 diabetes, severe obesity or cardiovascular diseases.

Human skeletal muscle sampling

Skeletal muscle biopsies were obtained from the vastus lateralis. Samples were collected under local anaesthesia (1% lidocaine) of the skin and superficial muscle fascia, using the Bergström technique (Bergström, 1962) with a needle modified for suction. The biopsy was immediately dissected free of fat and connective tissue and divided into sections for measurements of mitochondrial respiration.

Skeletal muscle preparation

Both human and mouse skeletal muscle samples were immediately placed in ice-cold biopsy preservation solution containing 2.77 mM CaK_2EGTA buffer, 7.23 mM K_2EGTA buffer, 0.1 μM free calcium, 20 mM imidazole, 20 mM taurine, 50 mM 2-(*N*-morpholino)ethanesulfonic acid hydrate (K-Mes), 0.5 mM dithiothreitol, 6.56 mM $MgCl_2.6H_2O$, 5.77 mM ATP and 15 mM phosphocreatine (pH 7.1). Muscle samples were then gently dissected with either a pair of fine-tipped forceps or the tip of two 18-gauge needles for murine and human skeletal muscle samples, respectively, achieving a high degree of fibre separation that was verified microscopically. Chemical permeabilization was carried out by incubation in 2 ml of biopsy preservation solution with saponin (50 μg ml^{-1}) for 30 min at 4°C (Kuznetsov *et al.* 2004). Finally, samples were washed with a mitochondrial respiration medium 05 (MiR05) containing 0.5 mM EGTA, 3 mM $MgCl_2.6H_2O$, 60 mM potassium lactobionate, 20 mM taurine, 10 mM KH_2P0_4, 20 mM Hepes, 110 mM sucrose and 1 g l^{-1} bovine serum albumin (pH 7.1) for 10 min at 4°C.

Mitochondrial respiration measurements

Muscle bundles were blotted dry and measured for wet weight in a balance-controlled scale (XS205 DualRange Analytical Balance; Mettler-Toledo AG, Greifensee, Switzerland), at constant relative humidity in order to provide hydration consistency as well as stability of weight measurements. Respiration measurements were performed in mitochondrial respiration medium 06 (MiR06; MiR05 + catalase 280 IU ml^{-1}). Measurements of oxygen consumption were performed at 37°C using the high-resolution Oxygraph-2k (Oroboros, Innsbruck, Austria), with all additions in each substrate, uncoupler and inhibitor titration protocol being added in series. Standardized instrumental calibrations were performed to correct for back diffusion of oxygen into the chamber from the various components, leak from the exterior, oxygen consumption by the chemical medium and oxygen consumption by the sensor. Oxygen flux was resolved by software allowing non-linear changes in the negative time derivative of the oxygen concentration signal (Oxygraph-2k; Oroboros). All experiments were carried out in a hyperoxygenated environment to prevent any potential oxygen diffusion limitation.

Respiratory titration protocol

The titration protocol was specific to the examination of individual aspects of respiratory control through a sequence of coupling and substrate states induced via separate titrations. All respirometric analyses were made in duplicate, and all titrations were added in series as presented. The concentrations of substrates, uncouplers and inhibitors used were based on prior experiments conducted for optimization of the titration protocols (Jacobs *et al.* 2011, 2012; Jacobs & Lundby, 2012).

Leak respiration in the absence of adenylates (L_N) was induced with the addition of malate (2 mM) and octanoyl carnitine (0.2 mM). The L_N state represents the resting oxygen consumption of an unaltered and intact electron transport system free of adenylates.

Maximal electron flow through electron-transferring flavoprotein (ETF) and fatty acid oxidative capacity (P_{ETF}) were both determined following the addition of ADP (5 mM). In the P_{ETF} state, the ETF-linked transfer of electrons requires the metabolism of acetyl-CoA, hence the addition of malate, in order to facilitate convergent electron flow into the Q-junction from both CI and ETF, allowing β-oxidation to proceed. The contribution of electron flow through CI is far below capacity and so here the rate-limiting metabolic branch is electron transport through ETF such that malate + octanoyl carnitine + ADP-stimulated respiration is representative of, rather than specific to, electron capacity through ETF (Eaton *et al.* 1996; Saks *et al.* 1998; Gnaiger, 2009; Pesta & Gnaiger, 2011; Pesta *et al.* 2011).

Submaximal state 3 respiratory capacity specific to CI (P_{CI}) was induced following the additions of

pyruvate (5 mM) and glutamate (10 mM). Maximal state 3 respiration, oxidative phosphorylation capacity (P), was then induced with the addition of succinate (10 mM). Oxidative phosphorylation capacity demonstrates the capacity of a naturally intact electron transport system to catalyse a sequential set of redox reactions that are partially coupled to the production of ATP via ATP synthase. Oxidative phosphorylation capacity maintains an electrochemical gradient across the inner mitochondrial membrane that is dictated by the degree of coupling to the phosphorylation system (Gnaiger, 2009; Pesta & Gnaiger, 2011). This maximal state represents respiration that is resultant to saturating concentrations of ADP and substrate supply for both CI and CII. Convergent electron input to CI and CII provides higher respiratory values compared with the isolated respiration of either CI (pyruvate/glutamate + malate or glutamate + malate) or CII (succinate + rotenone; Rasmussen & Rasmussen, 2000; Gnaiger, 2009). Consequently, P presents more physiological relevance to the study of mitochondrial function (Brand & Nicholls, 2011) and is necessary to establish confirmation of a complete and intact electron transport system.

As an internal control for compromised integrity of the mitochondrial preparation, the mitochondrial outer membrane was assessed with the addition of cytochrome *c* (10 μM). There was no indication of mitochondrial damage, because the 3.5, 2.1, 5.5 and –0.4% change in mouse $QUAD_M$, SOL_M, $GAST_M$ and $QUAD_H$ respiration, respectively, was either below or within the accepted 5–15% elevation in respiration following exogenous cytochrome *c*, verifying integrity of the outer mitochondrial membrane (Kuznetsov *et al.* 2008).

Phosphorylative restraint of electron transport was assessed by uncoupling ATP synthase (complex V) from the electron transport system with the titration of the proton ionophore, carbonyl cyanide *p*-(trifluoromethoxy) phenylhydrazone (FCCP; 0.5 μM per addition up to optimal concentrations ranging from 1.5 to 3 μM), reaching electron transport system (ETS) capacity. In the ETS respiratory state, the inner mitochondrial membrane potential is completely collapsed, with an open transmembrane proton circuit. The uninhibited flow of electrons through the respiratory system can therefore serve indirectly as an indication of maximal mitochondrial membrane potential.

Finally, rotenone (0.5 μM) and antimycin A (2.5 μM) were added, in sequence, to terminate respiration by inhibiting CI and complex III (CIII; cytochrome bc_1 complex), respectively. With CI inhibited, electron flow is specific to CII, providing submaximal state 3 respiration through CII (P_{CII}). There are negligible differences in P_{CII} when measured with or without a prior addition of FCCP (Jacobs *et al.* 2012), because the capacity for electron flow through CII is much less than that of CIII and complex IV (CIV; cytochrome *c* oxidase), and thus is rate limiting (Gnaiger, 2009). Inhibition of respiration with antimycin A then allows for the determination and correction of residual oxygen consumption, indicative of non-mitochondrial oxygen consumption in the chamber.

Citrate synthase activities

Citrate synthase (CS) activities were assayed in homogenates of the skeletal muscle samples used in respiration measurements. The contents of the Oxygraph-2k chambers (2 ml each) were removed after each respiration experiment and washed once with 2 ml of MiR05. One per cent Triton X-100 and 2 μl of a protease inhibitor cocktail (Sigma Aldrich catalogue no. 539134) were added to the combined solutions (content and wash) and then homogenized for 30 s with a T10 basic ULTRA-TURRAX® homogenizer near maximal speed (setting 4). The homogenate was then centrifuged for 15 min at 4°C, and the supernatant was removed, frozen in liquid nitrogen and stored at –80°C. As has been previously described (Srere, 1969), CS activity was measured fluorometrically at 412 nm and 25°C (Citrate Synthase Assay Kit; Sigma-Aldrich), according to the manufacturer.

Muscle lysate preparation

Muscle tissue ($QUAD_M$, SOL_M and $GAST_M$) was collected from a subgroup of mice ($n = 4$) to measure the protein expression of several mitochondria-specific proteins and compare quantification of those with our measure of CS activity to establish its validity as a biomarker of mitochondrial content in mouse skeletal muscle. The muscle samples were homogenized (Qiagen Tissuelyser II, Retsch, Haan, Germany) in a fresh batch of buffer containing the following: 10% glycerol, 20 mM sodium pyrophosphate, 150 mM NaCl, 50 mM Hepes (pH 7.5), 1% NP-40, 20 mM β-glycerophosphate, 2 mM Na_3VO_4, 10 mM NaF, 2 mM phenylmethylsulfonyl fluoride, 1 mM EDTA (pH 8.0), 1 mM EGTA (pH 8.0), 10 μg ml^{-1} aprotinin, 10 μg ml^{-1} leupeptin and 3 mM benzamidine. Afterwards, samples were rotated end over end for 1 h at 4°C and centrifuged at 16,500*g* for 30 min at 4°C, and the supernatant (lysate) was used for further analysis. The total protein concentration in each sample was determined by a bovine serum albumin standard kit (Pierce, Rockford, IL, USA), and samples were mixed with a modified 6× Laemmli buffer [7 ml 0.5 M Tris base (pH 6.8), 3 ml glycerol, 0.93 g dithiothreitol, 1 g SDS and 1.2 mg Bromophenol blue].

SDS-PAGE and Western blotting

Methods have been described in detail previously (Nordsborg *et al.* 2008, 2012; Thomassen *et al.* 2011). Equal amounts (10 μg) of total muscle lysate proteins, determined during optimization of the different antibodies, were loaded in each well. Samples were loaded together with protein markers (Precision Plus All Blue and Dual Colour; Bio-Rad Laboratories, Hercules, CA, USA) on precasted gels (Bio-Rad Laboratories). Proteins were separated by SDS-PAGE and semi-dry transferred to a polyvinylidene fluoride membrane (Millipore, Billerica, MA, USA). The membranes were blocked in either 2% skimmed milk or 3% bovine serum albumin in Tris-buffered saline, including 0.1% Tween 20 (TBST) before an overnight incubation in primary antibody at 4°C. Thereafter, membranes were washed in TBST and incubated for 1 h at room temperature in horseradish peroxidase-conjugated secondary antibody. Membranes were then washed three times for 15 min in TBST before the bands were visualized with ECL (Millipore) and recorded with a digital camera (ChemiDoc MP Imaging System; Bio-Rad). Quantification of the Western blot band intensity was done using the Image Lab software program (Bio-Rad) and determined as the total band intensity minus the background intensity. Primary antibodies were optimized by use of mouse muscle lysates to ensure that the amount of protein loaded would result in band signal intensities localized on the steep and linear part of a standard curve.

In order to determine changes in total protein expression, the following antibodies were used, with the localization of the quantified signal noted: 3-hydroxyacyl coenzyme *a* dehydrogenase (HAD), 83 kDa, polyclonal ab54477 (Abcam, Cambridge, UK); citrate synthase (CS), 48 kDa, polyclonal ab96600 (Abcam); mitochondrial complex IV subunit 4, (CIV), 16 kDa, monoclonal sc-58348 (Santa Cruz Biotechnology, Santa Cruz, CA, USA); and mitochondrial complex I subunit NDUFB8 (CI), 20 kDa (monoclonal ab110242), mitochondrial complex II, succinate dehydrogenase complex subunit B (CII), 30 kDa (monoclonal ab14714), mitochondrial complex III subunit core 2 (CIII), 45 kDa (monoclonal ab14745) and mitochondrial complex V ATP synthase subunit α (CV), 55 kDa (monoclonal ab14748), all four of which are included in the MitoProfile® Total OXPHOS Human WB Antibody Cocktail (ab110411; Abcam). The secondary antibodies used were horseradish peroxidase-conjugated goat anti-mouse and goat anti-rabbit (P-0447 and P-0448; Dako, Glostrup, Denmark).

All samples from the same muscle type were loaded on the same gel. The signal intensity from each muscle sample was normalized to the mean signal intensity of a human standard loaded together with the samples.

Data analysis

For all statistical evaluations, a P value of <0.05 was considered significant. Linear regression was used to calculate the strength of association between CS activity and the quantification of mitochondria-specific proteins from the tricarboxylic acid cycle, β-oxidation pathway and electron transport system across all types of murine skeletal muscles. Respiratory capacities, CS activity and indices of mitochondrial efficiency did not show a Gausian distribution; therefore a Kruskal–Wallis ANOVA and the Mann–Whitney U test were used to reveal differences between muscles. Pearson correlation coefficients were calculated for the strength of association between P and CS activity.

Results

Mass-specific respiration across mouse skeletal muscle

Differences in mass-specific respiratory capacity across different skeletal muscles in the mouse are presented in Fig. 1*A*. For all respiratory states, SOL_M was significantly ($P < 0.01$) greater than both $QUAD_M$ and $GAST_M$. The only difference observed between $QUAD_M$ and $GAST_M$ was in maximal fatty acid oxidation capacity, P_{ETF}, where $QUAD_M$ expressed a greater capacity ($P = 0.028$).

Mitochondrial respiratory capacity and content

Mass-specific respiration does not take into account differences in mitochondrial content. When controlling mass-specific respiration for mitochondrial content, the differences in respiratory capacities across all mouse skeletal muscles change (Fig. 1*B*). Specifically, both $QUAD_M$ and $GAST_M$ were greater than SOL_M during submaximal state 3 respiration through CI (P_{CI}; $P = 0.005$ and 0.001, respectively), maximal state 3 respiration (P; $P = 0.007$ and $P < 0.001$, respectively), electron transport system capacity (ETS; $P = 0.01$ and $P < 0.001$, respectively) and submaximal state 3 respiration through CII (P_{CII}; $P = 0.021$ and $P = 0.001$, respectively). Mitochondrial content correlates directly with overall respiratory capacity (Larsen *et al.* 2012). This is shown here, because maximal state 3 respiration, or oxidative phosphorylation capacity, P, strongly correlates ($r = 0.932$, $P < 0.001$) with CS activity across all mouse muscles (Fig. 1*C*). When analysing differences in CS activity across groups, SOL_M presents with more CS activity than any other skeletal muscle ($P < 0.001$). The only other difference was that CS activity in $GAST_M$ was less than in $QUAD_H$ ($P < 0.002$).

Mitochondria-specific respiration across mouse muscles

Although CS activity has been shown to correlate strongly with mitochondrial content in humans (Larsen *et al.* 2012) and also in horses (Hoppeler, 1990), it was necessary to establish this in mouse skeletal muscle. In order to validate measures of CS activity in mouse skeletal muscle, we correlated those values to quantification of mitochondrial enzymes from a subgroup of animals included in this study ($n = 4$). The quantification of all mitochondrial proteins analysed in $QUAD_M$, SOL_M and $GAST_M$ is

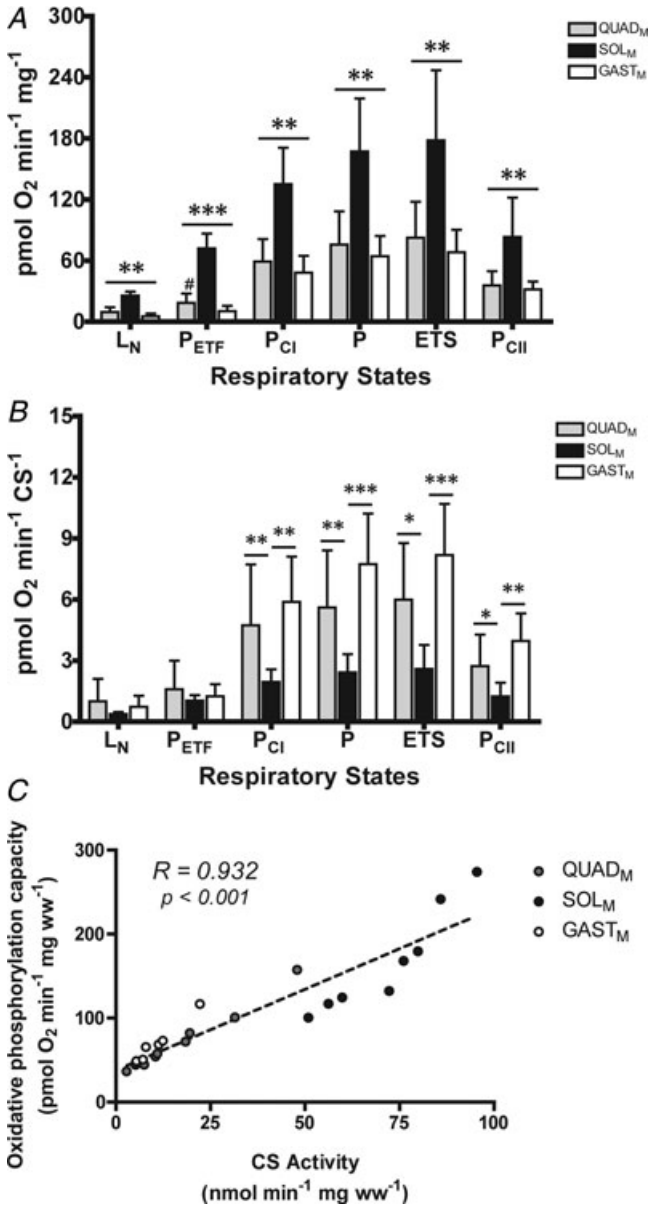

Figure 1. Comparison of respiratory capacity and control in mouse skeletal muscles
Mass-specific (*A*) and mitochondria-specific respiration (*B*) across mouse quadriceps ($QUAD_M$; grey bars), soleus (SOL_M; filled bars) and gastrocnemius ($GAST_M$; open bars). Abbreviations: L_N, leak respiration without adenylates; P, maximal state 3 respiration, i.e. oxidative phosphorylation capacity; P_{CI}, submaximal state 3 respiration through complex I (CI); P_{CII}, submaximal state 3 respiration through complex II (CII); and P_{ETF}, maximal fatty acid oxidation. Data are presented as means + SD. $^{*}P \leq 0.05$, $^{**}P \leq 0.01$ and $^{***}P \leq 0.001$. #Significant difference from $GAST_M$, $P < 0.05$. *C*, Pearson correlation of maximal oxidative phosphorylation system capacity, maximal state 3 respiration (P), *versus* citrate synthase (CS) activity. Citrate synthase activity (*x*-axis) is plotted against P (*y*-axis) for all mouse skeletal muscles. The grey circles represent $QUAD_M$, the filled circles SOL_M and the open circles $GAST_M$. $r = 0.932$, $P < 0.001$.

illustrated in the Supplemental material (Fig. S1). All quantifications of mitochondrial proteins correlated strongly with measures of CS activity (Supplemental material, Fig. S1), establishing its use as a valid biomarker of mitochondrial content in mouse skeletal muscle.

Mitochondrial function in mouse quadriceps *versus* human quadriceps

Mass-specific respirometric comparisons of $QUAD_M$ differed from its human counterpart during P_{ETF} ($P = 0.007$), P_{CI} ($P = 0.05$), P ($P = 0.015$) and ETS ($P = 0.002$) respiratory states (Fig. 2*A*). When controlling for mitochondrial content, the only difference between $QUAD_M$ and $QUAD_H$ was observed at ETS ($P = 0.038$; Fig. 2*B*).

Mitochondrial function in mouse soleus *versus* human quadriceps

Mass-specific respiratory values from SOL_M and $QUAD_H$ mitochondria are presented in Fig. 3*A*. They differed during leak respiration in absence of adenylates (L_N; $P < 0.001$), P_{ETF} ($P < 0.001$), P_{CI} ($P = 0.005$) and P_{CII} ($P = 0.002$). When controlling for mitochondrial content, the differences between SOL_M and $QUAD_H$ were observed at P_{ETF} ($P = 0.002$), P_{CI} ($P < 0.001$), P ($P < 0.001$) and ETS ($P < 0.001$) respiratory states (Fig. 3*B*).

Mitochondrial function in mouse gastrocnemius *versus* human quadriceps

Mass-specific differences for all respiratory states except P_{CII} were lower in $GAST_M$ when compared with $QUAD_H$ (Fig. 4*A*; L_N, $P = 0.05$; P_{ETF}, $P < 0.001$; P_{CI}, $P = 0.003$; P, $P = 0.003$; and ETS, $P < 0.001$). When controlling for mitochondrial content, the only differences between $GAST_M$ and $QUAD_H$ were at P_{CI} ($P = 0.05$) and P_{CII} ($P = 0.007$) respiratory states (Fig. 4*B*).

Mitochondrial coupling control

The leak control ratio during β-oxidation (LCR_{ETF}), representing the electron coupling control during fat oxidation, differed between $QUAD_M$ and SOL_M ($P = 0.015$) and between $QUAD_M$ and $QUAD_H$ ($P = 0.005$). The phosphorylation system control ratio (PSCR) did not differ between any mouse muscles (Fig. 5); however, all the mouse muscles presented with a higher PSCR than the human muscle ($P < 0.001$).

Discussion

The aim of this study was to analyse respiratory capacity and control in several mouse muscles and to compare and contrast those values with skeletal muscle mitochondrial function measured in muscle from young and healthy human subjects. We have several main findings, as follows: (i) qualitative differences in mitochondrial function exist between mouse skeletal muscles; (ii) respiratory capacity in young, healthy mouse skeletal muscle does correspond well to that of young, healthy human skeletal muscle; and (iii) in contrast to our hypothesis, mitochondrial function of the $QUAD_M$, not SOL_M, more closely resembles that of human skeletal muscle.

There is discussion on whether the respiratory capacity of skeletal muscle depends solely on mitochondrial content or whether differences exist across skeletal muscles with varying biochemical make-up (Picard *et al.* 2012). There is some evidence in support of the supposition that differences in oxidative potential between skeletal muscles can be accounted for by the mitochondrial volume density between the muscles (Hoppeler *et al.* 1987; Schwerzmann *et al.* 1989), although these studies were limited either by measuring P_{CI} and P_{CII} only individually, but not collectively, in preparations of isolated mitochondria or by perfusion limitations to the skeletal muscle. Other evidence suggests, as do the results presented here, that a respiratory difference between oxidative and glycolytic muscle mitochondria does exist when taking into account mitochondrial content (Jackman & Willis, 1996; Picard *et al.* 2008). All data reporting differences between oxidative and glycolytic muscles report a higher respiratory capacity per mitochondrion in glycolytic muscle (Jackman & Willis, 1996; Picard *et al.* 2008). Respiratory differences across skeletal muscle fibre types have also been shown in human subjects using *in vivo* imaging techniques (Amara *et al.* 2007; Conley *et al.* 2007). Here we maintain that there are differences in respiratory capacity per mitochondrion across different skeletal muscles and that the more glycolytic muscle possesses greater respiratory capacity for a given mitochondrial content (Fig. 1*B*).

The mechanism(s) explaining these functional differences across skeletal muscle fibre types are largely unknown. Mitochondria do, however, vary morphometrically between fibre types, with mitochondria of fast-twitch muscles possessing a thinner and longer reticular network and mitochondria of slow-twitch muscles expressing a thicker and more truncated reticulum (Ogata & Yamasaki, 1997). The mitochondria expressed in different fibre types are also sometimes subjected to very a different metabolic strain. Glycogen stores are markedly greater in fast-twitch glycolytic muscles when compared with slow-twitch oxidative muscles (Greenhaff *et al.* 1991; Tsintzas *et al.* 1995),

as are the maximal rates of glycogenolysis within each respective muscle type (Greenhaff *et al.* 1991). The greater respiratory capacity per mitochondrion in glycolytic muscle is necessary and may be explained by the greater glycolytic strain per unit mitochondria during intense to maximal exertion. Biochemical protein expression supports this idea, because several mitochondrial enzymes directly involved in the function of the tricarboxylic acid cycle and electron transport chain, e.g. NADH dehydrogenase, have been reported to possess greater expression in glycolytic compared with oxidative skeletal muscle (Glancy & Balaban, 2011).

Normalization of respiration plays a large role in whether or not differences are observed between oxidative and glycolytic fibres; oxidative fibres express greater respiratory capacity when normalized to tissue weight (Fig. 1*A*), because they possess considerably higher mitochondrial content (Fig. 1*C*). This is in

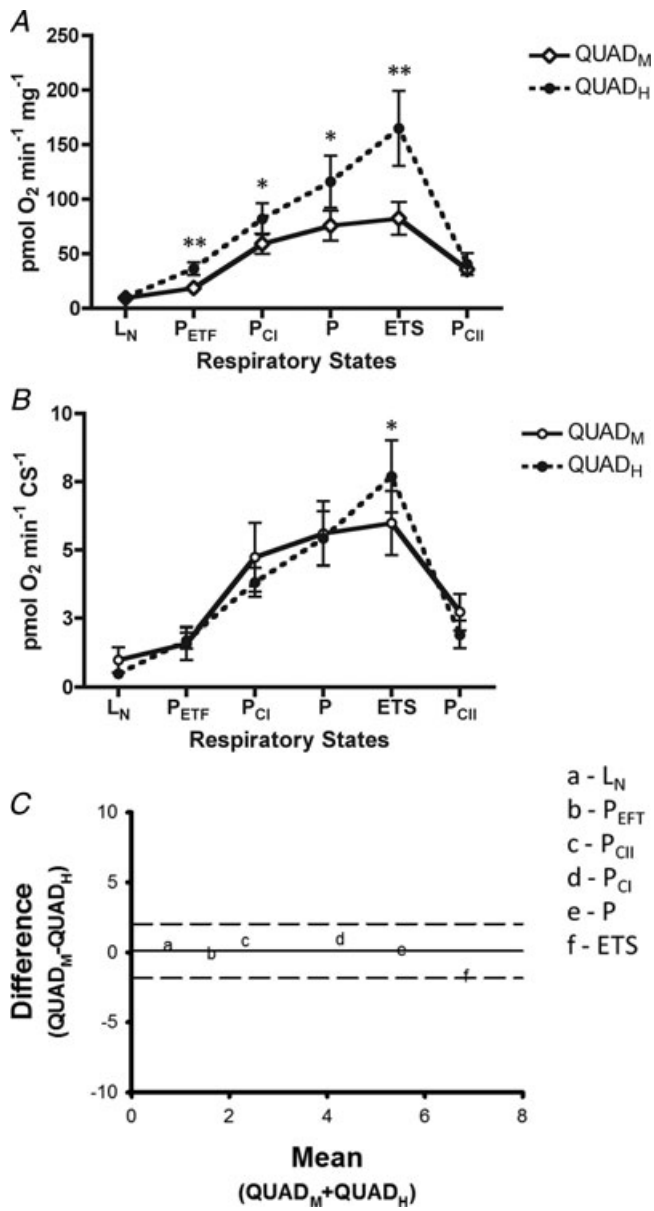

Figure 2. Respiratory capacity and control between mouse quadriceps ($QUAD_M$) and human quadriceps ($QUAD_H$)
Mass-specific (*A*) and mitochondria-specific respiration (*B*). Data are presented as means + SD. $^{*}P \leq 0.05$ and $^{**}P \leq 0.01$. *C*, Bland–Altman plots representing the mean difference and the limit of agreement between $QUAD_M$ and $QUAD_H$ across respiratory states. The continuous line represents the mean of the differences between $QUAD_M$ and $QUAD_H$ and the dashed lines represent the level of agreement (mean $\pm$ 2SD). The smaller the range between these two limits, the better the agreement.

agreement with previous reports (Ponsot *et al.* 2005; Picard *et al.* 2008). Normalization to mitochondrial content is required for comparison of true differences in respiratory capacity between skeletal muscles. Respirometric analysis of mitochondria isolated from rat soleus, extensor digitorum longus, gastrocnemius and tibialis anterior found no difference in respiratory capacity in subsarcolemmal or intermyofibrillar populations when normalized to mitochondrial protein content (Yajid *et al.* 1998). Mitochondrial isolation, however, disrupts the united heterogeneous mitochondrial reticulum, resulting in unnaturally circular and disconnected organelles (Schwerzmann *et al.* 1989; Picard *et al.* 2011). This carries the risk of contaminating the isolated fractions

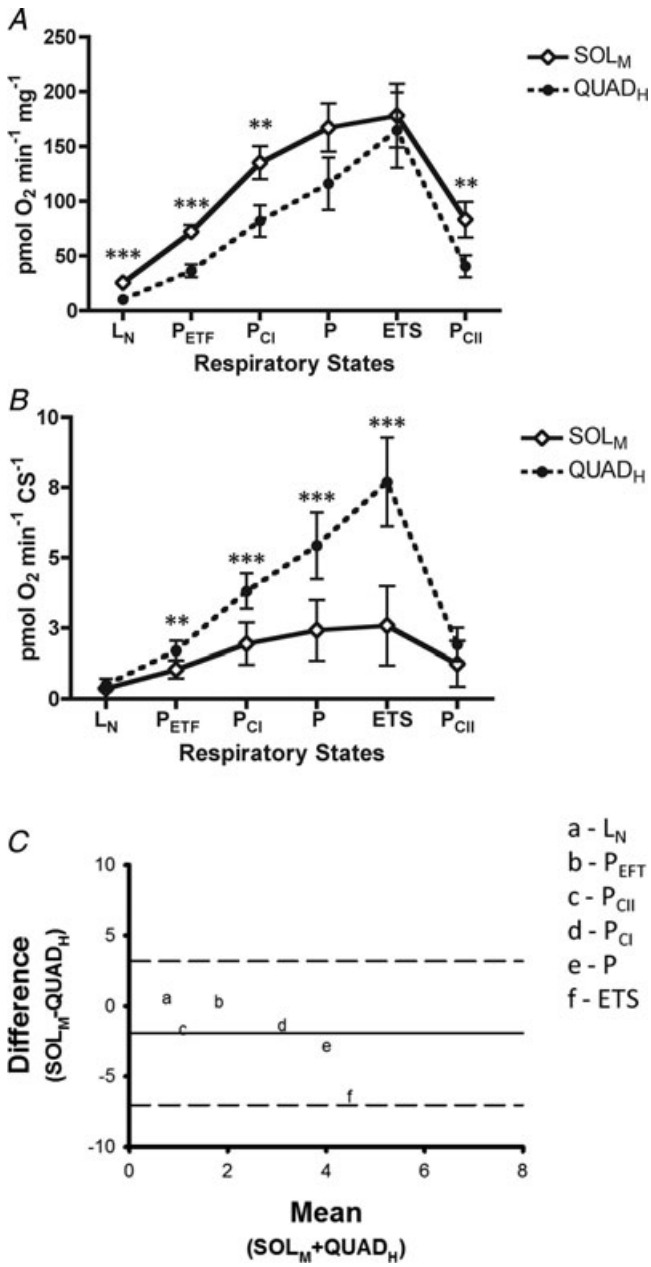

Figure 3. Respiratory capacity and control between mouse soleus (SOL_M) and human quadriceps ($QUAD_H$)
Mass-specific (*A*) and mitochondria-specific respiration (*B*). Data are presented as means + SD. $^{**}P \leq 0.01$ and $^{***}P \leq 0.001$. *C*, Bland–Altman plots representing the mean difference and the limit of agreement between SOL_M and $QUAD_H$ across respiratory states. The continuous line represents the mean of the differences between SOL_M and $QUAD_H$ and the dashed lines represent the level of agreement (mean ± 2SD). The smaller the range between these two limits, the better the agreement.

with proteins not native to the mitochondria (Chretien *et al.* 1995; Picard *et al.* 2011), losing mitochondria-specific contents (Brooks, 2002; Brooks & Hashimoto, 2007; Picard *et al.* 2011) and modifying overall function (Pande & Blanchaer, 1970; Benz, 1994; Saks *et al.* 1998, 2010; Villani *et al.* 1998; Kunz *et al.* 2000; Milner *et al.* 2000; Kuznetsov *et al.* 2008; Picard *et al.* 2010). Moreover, respirometric normalization to mitochondrial protein following mitochondrial isolation has since been rebutted, because it does not correlate with the total area of the cristae (Leary *et al.* 2003). Respirometric normalization to a biomarker of mitochondrial content, such as CS, which is different between muscles, was not analysed (Yajid *et al.* 1998). In human skeletal muscle, CS activity can serve as a valid representative biomarker of mitochondrial volume density, total cristae area and respiratory capacity (Larsen

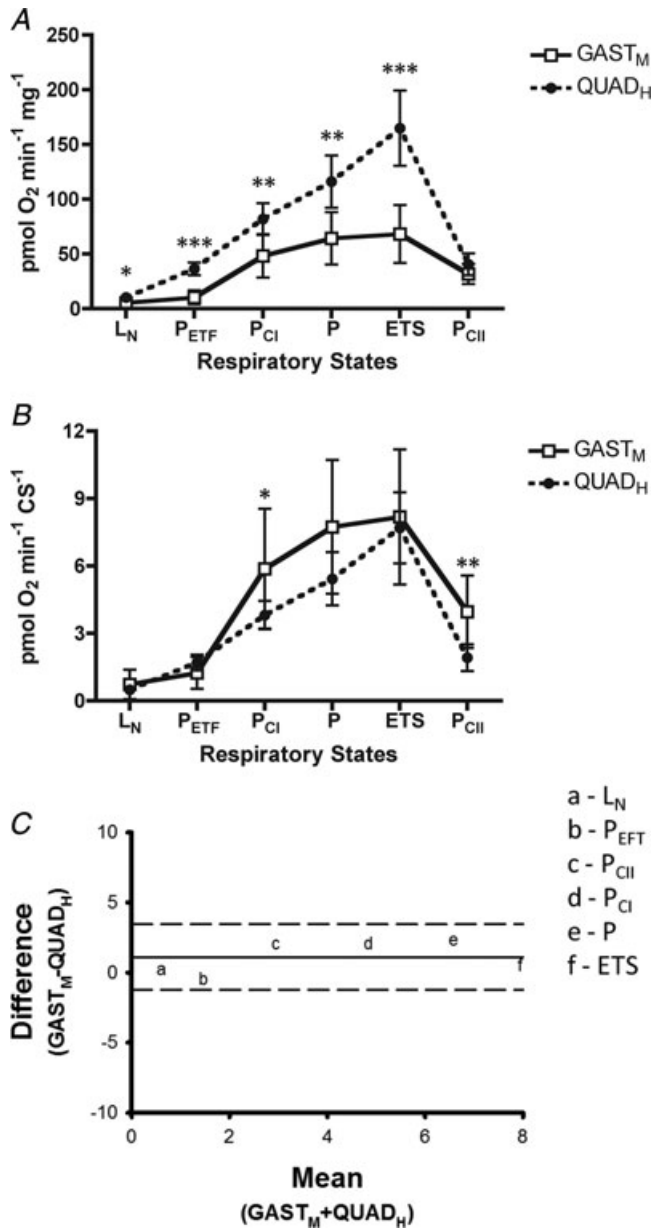

Figure 4. Respiratory capacity and control between mouse gastrocnemius ($GAST_M$) and human quadriceps ($QUAD_H$)
Mass-specific (*A*) and mitochondria-specific respiration (*B*). Data are presented as means + SD. $^{*}P \leq 0.05$, $^{**}P \leq 0.01$ and $^{***}P \leq 0.001$. *C*, Bland–Altman plots representing the mean difference and the limit of agreement between $GAST_M$ and $QUAD_H$ across respiratory states. The continuous line represents the mean of the differences between $GAST_M$ and $QUAD_H$ and the dashed lines represent the level of agreement (mean ± 2SD). The smaller the range between these two limits, the better the agreement.

et al. 2012). We also validate CS activity as a representative biomarker of mitochondrial content in mouse skeletal muscle, because there were strong correlations with CS activity and quantification of all mitochondrial proteins analysed (Supplemental material, Fig. S1). An additional benefit to the use of measurements of CS activity is that they can be made from the same skeletal muscle preparation used to collect respirometric values (Picard *et al.* 2008; Larsen *et al.* 2012), as was done in the present study.

The ability to use animal models for human mitochondrial function is important, because mitochondria are intimately associated with both health and disease. Use of the mouse as a representative model of human mitochondrial function, however, has come into question (Lemieux & Warren, 2012). Differences in molecular profiles between mouse and human skeletal muscle indirectly support these claims. However, the assertion that mouse mitochondrial function deviates greatly from that in the human has never empirically been tested until now. Using saponin-permeabilized skeletal muscle preparations from $QUAD_M$ and $QUAD_H$, we show that the differences in respiratory control across species are minor or negligible (Fig. 2*B*). In contrast to isolated mitochondrial preparations, this specific mitochondrial preparation allows for direct access to skeletal muscle mitochondria while preserving the cytocellular ultrastructure (Lin *et al.* 1990; Saks *et al.* 1991, 1998; Kuznetsov *et al.* 2008; Gnaiger, 2009; Pesta & Gnaiger, 2011; Picard *et al.* 2011) as well as subcellular interactions (Veksler *et al.* 1987; Lin *et al.* 1990; Saks *et al.* 1998; Milner *et al.* 2000; Kuznetsov *et al.* 2008; Picard *et al.* 2011). Cellular bioenergetics and metabolic channelling are reliant upon these characteristics (Saks *et al.* 1998; Kay *et al.* 2000; Kuznetsov *et al.* 2008; Gnaiger, 2009). Accordingly, this specific mitochondrial preparation serves as the best model in which to examine differences between skeletal muscle types and also to compare and contrast function across species.

In contrast to our hypothesis, it was respiratory capacity and control of the $QUAD_M$, not SOL_M, that better represents human skeletal muscle mitochondrial function (Figs 2*B versus* 3*B*). These data also refute previous reports that the SOL_M may serve as a better representative of human skeletal muscle based on molecular modelling (Kho *et al.* 2006). Bland–Altman plots further verified this finding (Figs 2*C*, 3*C* and 4*C*). These Bland–Altman plots are graphical representations of the differences between the respirometric analysis of mouse muscle and human muscle against the mean for each respective respiratory state. This method determines the mean difference (measurement bias) between the two measurements in question, as well as the 95% limit of agreement of the mean difference (2SD). The smaller the range between these two limits, the better the agreement.

It should be noted that mitochondrial electron coupling control during fat oxidation is more similar between SOL_M and $QUAD_H$ (Fig. 5). The LCR_{ETF} is determined from two respiratory states, a leak state (L_N) and a higher respiratory state (P_{EFT}). These corresponding states are paired by an identical substrate supply (malate + octanoyl carnitine). The ratio of these two states reflects electron coupling efficiency during fat oxidation, from a theoretical minimum of 0.0, indicating a fully coupled system, to a value of 1.0, representing a fully non-coupled (dyscoupled) system (Gnaiger, 2009). Thus, while $QUAD_M$ was most similar to $QUAD_H$ respiratory capacities, it may be more accurate to state that mouse skeletal muscles can provide a useful model to test hypotheses relating to human skeletal muscle with the caveat that species differences are real, very specific, different across muscle types, and must be considered before extrapolating directly to human skeletal muscle. We also confirmed that young, healthy mice may serve as representative models of mitochondrial performance in young, healthy and non-sedentary humans. The comorbidities of a sedentary, caged and *ad libitum*-fed lifestyle (Martin *et al.* 2010) do not appear to affect mitochondrial function within the first 8–10 weeks of life.

One difference that did exist between all mouse skeletal muscles and the human muscle was the PSCR. This is the ratio of maximal state 3 respiration to ETS capacity and represents the degree of constraint of the maximal oxidative phosphorylation capacity by the phosphorylation system or ATP synthase (Gnaiger, 2009). With no restriction, the PSCR approaches a ratio of 1.0, which we observed in all mouse muscles (Fig. 5), as seen in other studies (ter Veld *et al.* 2005; Aragonés *et al.* 2008). We observed that human skeletal muscle

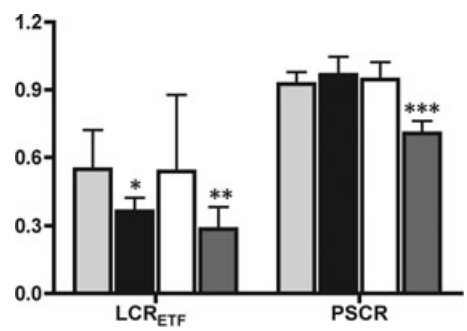

Figure 5. Mitochondrial coupling control across all groups
Leak-control ratios (LCRs) for the coupling control of electron transport through the electron-transferring flavoprotein (ETF) during β-oxidation (LCR_{ETF}) and phosphorylation system control ratio (PSCR) across mouse quadriceps ($QUAD_M$; light grey bars), mouse soleus (SOL_M; dark grey bars), mouse gastrocnemius ($GAST_M$; open bars) and human quadriceps ($QUAD_H$; filled bars). Data are presented as means + SD. $^*P \leq 0.05$, $^{**}P \leq 0.01$ from $QUAD_M$. $^{***}P < 0.001$ from all mouse skeletal muscle.

presented with an average PSCR of 0.71, which is also comparable to other reported values (Boushel *et al.* 2007). A ratio less than 1.0, as observed in humans, suggests that electron transport through complexes I–IV is limited by ADP phosphorylation. When facilitating non-coupled respiration with the proton ionophore FCCP by collapsing the electron gradient prior to phosphorylation, a higher electron transport and attendant respiration is reached ($QUAD_H$ respiration; Fig. 2*B*). Oxidative phosphorylation capacity (P) is more than capable of utilizing the oxygen delivered during maximal whole-body exercise (Boushel *et al.* 2011), where oxygen delivery is limiting. Thus, the excess capacity for electron transport following uncoupling in human skeletal muscle mitochondria possibly serves a functional role during exercise in isolated muscle groups where maximal work is not limited by oxygen supply (Andersen & Saltin, 1985). The functional role of an excess electron transport capacity in human skeletal muscle mitochondria merits further investigation.

Conclusion

If differences in murine and human mitochondrial function did exist then it would be both difficult and cavalier to apply results collected from mice to a larger and different human population, particularly if neither the group sampled nor the population was clearly defined. Here we discriminate between skeletal muscle mitochondrial function in mice and humans. We provide evidence disproving any excessive discordance or discrepancy that has been claimed to exist between mouse and human mitochondria unless specifically examining the phosphorylative restraint of ATP synthase on oxidative phosphorylation (Lemieux & Warren, 2012). Specifically, young, healthy mouse quadriceps serves as a suitable representative for mitochondrial function in young, healthy human vastus lateralis. This allows for more assurance when progressing from descriptive to inferential statistics between healthy young mouse and human mitochondria.

References

Amara CE, Shankland EG, Jubrias SA, Marcinek DJ, Kushmerick MJ & Conley KE (2007). Mild mitochondrial uncoupling impacts cellular aging in human muscles *in vivo*. *Proc Natl Acad Sci U S A* **104**, 1057–1062.

Andersen P & Saltin B (1985). Maximal perfusion of skeletal muscle in man. *J Physiol* **366**, 233–249.

Aragonés J, Schneider M, Van Geyte K, Fraisl P, Dresselaers T, Mazzone M *et al.* (2008). Deficiency or inhibition of oxygen sensor Phd1 induces hypoxia tolerance by reprogramming basal metabolism. *Nat Genet* **40**, 170–180.

Benz R (1994). Permeation of hydrophilic solutes through mitochondrial outer membranes: review on mitochondrial porins. *Biochim Biophys Acta* **1197**, 167–196.

Bergström J (1962). Muscle electrolytes in man. *Scand J Clin Lab Invest* **68**, 1–110.

Bernstein D (2003). Exercise assessment of transgenic models of human cardiovascular disease. *Physiol Genomics* **13**, 217–226.

Boushel R, Gnaiger E, Calbet JA, Gonzalez-Alonso J, Wright-Paradis C, Sondergaard H, Ara I, Helge JW & Saltin B (2011). Muscle mitochondrial capacity exceeds maximal oxygen delivery in humans. *Mitochondrion* **11**, 303–307.

Boushel R, Gnaiger E, Schjerling P, Skovbro M, Kraunsøe R & Dela F (2007). Patients with type 2 diabetes have normal mitochondrial function in skeletal muscle. *Diabetologia* **50**, 790–796.

Brand MD & Nicholls DG (2011). Assessing mitochondrial dysfunction in cells. *Biochem J* **435**, 297–312.

Brooks GA (2002). Lactate shuttle – between but not within cells? *J Physiol* **541**, 333–334.

Brooks GA & Hashimoto T (2007). Investigation of the lactate shuttle in skeletal muscle mitochondria. *J Physiol* **584**, 705–706; author reply 707–708.

Chomentowski P, Coen PM, Radiková Z, Goodpaster BH & Toledo FG (2011). Skeletal muscle mitochondria in insulin resistance: differences in intermyofibrillar *versus* subsarcolemmal subpopulations and relationship to metabolic flexibility. *J Clin Endocrinol Metab* **96**, 494–503.

Chretien D, Pourrier M, Bourgeron T, Séné M, Rötig A, Munnich A & Rustin P (1995). An improved spectrophotometric assay of pyruvate dehydrogenase in lactate dehydrogenase contaminated mitochondrial preparations from human skeletal muscle. *Clin Chim Acta* **240**, 129–136.

Conley KE, Amara CE, Jubrias SA & Marcinek DJ (2007). Mitochondrial function, fibre types and ageing: new insights from human muscle *in vivo*. *Exp Physiol* **92**, 333–339.

Demetrius L (2006). Aging in mouse and human systems: a comparative study. *Ann N Y Acad Sci* **1067**, 66–82.

Desai KH, Sato R, Schauble E, Barsh GS, Kobilka BK & Bernstein D (1997). Cardiovascular indexes in the mouse at rest and with exercise: new tools to study models of cardiac disease. *Am J Physiol Heart Circ Physiol* **272**, H1053–H1061.

Eaton S, Bartlett K & Pourfarzam M (1996). Mammalian mitochondrial β-oxidation. *Biochem J* **320**, 345–357.

Garland T Jr, Schutz H, Chappell MA, Keeney BK, Meek TH, Copes LE, Acosta W, Drenowatz C, Maciel RC, van Dijk G, Kotz CM & Eisenmann JC (2011). The biological control of voluntary exercise, spontaneous physical activity and daily energy expenditure in relation to obesity: human and rodent perspectives. *J Exp Biol* **214**, 206–229.

Glancy B & Balaban RS (2011). Protein composition and function of red and white skeletal muscle mitochondria. *Am J Physiol Cell Physiol* **300**, C1280–C1290.

Gnaiger E (2009). Capacity of oxidative phosphorylation in human skeletal muscle: new perspectives of mitochondrial physiology. *Int J Biochem Cell Biol* **41**, 1837–1845.

Greenhaff PL, Ren JM, Söderlund K & Hultman E (1991). Energy metabolism in single human muscle fibers during contraction without and with epinephrine infusion. *Am J Physiol Endocrinol Metab* **260**, E713–E718.

Hoppeler H (1990). *The Dynamic State of Muscle Fibers*. Walter de Gruyter, Berlin.

Hoppeler H, Hudlicka O & Uhlmann E (1987). Relationship between mitochondria and oxygen consumption in isolated cat muscles. *J Physiol* **385**, 661–675.

Jackman MR & Willis WT (1996). Characteristics of mitochondria isolated from type I and type IIb skeletal muscle. *Am J Physiol Cell Physiol* **270**, C673–C678.

Jacobs HT (2003). The mitochondrial theory of aging: dead or alive? *Aging Cell* **2**, 11–17.

Jacobs RA & Lundby C. (2012). Mitochondria express enhanced quality as well as quantity in association with aerobic fitness across recreationally active individuals up to elite athletes. *J Appl Physiol*, doi:10.1152/japplphysiol.01081.2012.

Jacobs RA, Rasmussen P, Siebenmann C, Díaz V, Gassmann M, Pesta D, Gnaiger E, Nordsborg NB, Robach P & Lundby C (2011). Determinants of time trial performance and maximal incremental exercise in highly trained endurance athletes. *J Appl Physiol* **111**, 1422–1430.

Jacobs RA, Siebenmann C, Hug M, Toigo M, Meinild AK & Lundby C (2012). Twenty-eight days at 3454-m altitude diminishes respiratory capacity but enhances efficiency in human skeletal muscle mitochondria. *FASEB J* **26**, 5192–5200.

Kay L, Nicolay K, Wieringa B, Saks V & Wallimann T (2000). Direct evidence for the control of mitochondrial respiration by mitochondrial creatine kinase in oxidative muscle cells *in situ*. *J Biol Chem* **275**, 6937–6944.

Kho AT, Kang PB, Kohane IS & Kunkel LM (2006). Transcriptome-scale similarities between mouse and human skeletal muscles with normal and myopathic phenotypes. *BMC Musculoskelet Disord* **7**, 23.

Kunz WS, Kudin A, Vielhaber S, Elger CE, Attardi G & Villani G (2000). Flux control of cytochrome *c* oxidase in human skeletal muscle. *J Biol Chem* **275**, 27741–27745.

Kuznetsov AV, Schneeberger S, Seiler R, Brandacher G, Mark W, Steurer W, Saks V, Usson Y, Margreiter R & Gnaiger E (2004). Mitochondrial defects and heterogeneous cytochrome *c* release after cardiac cold ischemia and reperfusion. *Am J Physiol Heart Circ Physiol* **286**, H1633–H1641.

Kuznetsov AV, Veksler V, Gellerich FN, Saks V, Margreiter R & Kunz WS (2008). Analysis of mitochondrial function *in situ* in permeabilized muscle fibers, tissues and cells. *Nat Protoc* **3**, 965–976.

Larsen S, Nielsen J, Hansen CN, Nielsen LB, Wibrand F, Stride N, Schroder HD, Boushel R, Helge JW, Dela F & Hey-Mogensen M (2012). Biomarkers of mitochondrial content in skeletal muscle of healthy young human subjects. *J Physiol* **590**, 3349–3360.

Leary SC, Lyons CN, Rosenberger AG, Ballantyne JS, Stillman J & Moyes CD (2003). Fiber-type differences in muscle mitochondrial profiles. *Am J Physiol Regul Integr Comp Physiol* **285**, R817–R826.

Lemieux H & Warren BE (2012). An animal model to study human muscular diseases involving mitochondrial oxidative phosphorylation. *J Bioenerg Biomembr* **44**, 503–512.

Lin A, Krockmalnic G & Penman S (1990). Imaging cytoskeleton–mitochondrial membrane attachments by embedment-free electron microscopy of saponin-extracted cells. *Proc Natl Acad Sci U S A* **87**, 8565–8569.

Lowell BB & Shulman GI (2005). Mitochondrial dysfunction and type 2 diabetes. *Science* **307**, 384–387.

Martin B, Ji S, Maudsley S & Mattson MP (2010). "Control" laboratory rodents are metabolically morbid: why it matters. *Proc Natl Acad Sci U S A* **107**, 6127–6133.

Miller BF, Robinson MM, Bruss MD, Hellerstein M & Hamilton KL (2012). A comprehensive assessment of mitochondrial protein synthesis and cellular proliferation with age and caloric restriction. *Aging Cell* **11**, 150–161.

Milner DJ, Mavroidis M, Weisleder N & Capetanaki Y (2000). Desmin cytoskeleton linked to muscle mitochondrial distribution and respiratory function. *J Cell Biol* **150**, 1283–1298.

Nordsborg N, Ovesen J, Thomassen M, Zangenberg M, Jøns C, Iaia FM, Nielsen JJ & Bangsbo J (2008). Effect of dexamethasone on skeletal muscle Na^+,K^+ pump subunit specific expression and K^+ homeostasis during exercise in humans. *J Physiol* **586**, 1447–1459.

Nordsborg NB, Siebenmann C, Jacobs RA, Rasmussen P, Diaz V, Robach P & Lundby C (2012). Four weeks of normobaric "live high-train low" do not alter muscular or systemic capacity for maintaining pH and K^+ homeostasis during intense exercise. *J Appl Physiol* **112**, 2027–2036.

Ogata T & Yamasaki Y (1997). Ultra-high-resolution scanning electron microscopy of mitochondria and sarcoplasmic reticulum arrangement in human red, white, and intermediate muscle fibers. *Anat Rec* **248**, 214–223.

Paglialunga S, van Bree B, Bosma M, Valdecantos MP, Amengual-Cladera E, Jörgensen JA, van Beurden D, den Hartog GJ, Ouwens DM, Briedé JJ, Schrauwen P & Hoeks J (2012). Targeting of mitochondrial reactive oxygen species production does not avert lipid-induced insulin resistance in muscle tissue from mice. *Diabetologia* **55**, 2759–2768.

Pande SV & Blanchaer MC (1970). Preferential loss of ATP-dependent long-chain fatty acid activating enzyme in mitochondria prepared using Nagarse. *Biochim Biophys Acta* **202**, 43–48.

Pesta D & Gnaiger E (2011). High-resolution respirometry: OXPHOS protocols for human cell cultures and permeabilized fibers from small biopsies of human muscle. *Methods Mol Biol* **810**, 25–58.

Pesta D, Hoppel F, Macek C, Messner H, Faulhaber M, Kobel C, Parson W, Burtscher M, Schocke M & Gnaiger E (2011). Similar qualitative and quantitative changes of mitochondrial respiration following strength and endurance training in normoxia and hypoxia in sedentary humans. *Am J Physiol Regul Integr Comp Physiol* **301**, R1078–R1087.

Picard M, Csukly K, Robillard ME, Godin R, Ascah A, Bourcier-Lucas C & Burelle Y (2008). Resistance to Ca^{2+}-induced opening of the permeability transition pore differs in mitochondria from glycolytic and oxidative muscles. *Am J Physiol Regul Integr Comp Physiol* **295**, R659–R668.

Picard M, Hepple RT & Burelle Y (2012). Mitochondrial functional specialization in glycolytic and oxidative muscle fibers: tailoring the organelle for optimal function. *Am J Physiol Cell Physiol* **302**, C629–C641.

Picard M, Ritchie D, Wright KJ, Romestaing C, Thomas MM, Rowan SL, Taivassalo T & Hepple RT (2010). Mitochondrial functional impairment with aging is exaggerated in isolated mitochondria compared to permeabilized myofibers. *Aging Cell* **9**, 1032–1046.

Picard M, Taivassalo T, Gouspillou G & Hepple RT (2011). Mitochondria: isolation, structure and function. *J Physiol* **589**, 4413–4421.

Ponsot E, Zoll J, N'Guessan B, Ribera F, Lampert E, Richard R, Veksler V, Ventura-Clapier R & Mettauer B (2005). Mitochondrial tissue specificity of substrates utilization in rat cardiac and skeletal muscles. *J Cell Physiol* **203**, 479–486.

Rangarajan A & Weinberg RA (2003). Opinion: Comparative biology of mouse versus human cells: modelling human cancer in mice. *Nat Rev Cancer* **3**, 952–959.

Rasmussen UF & Rasmussen HN (2000). Human skeletal muscle mitochondrial capacity. *Acta Physiol Scand* **168**, 473–480.

Rennie MJ, Selby A, Atherton P, Smith K, Kumar V, Glover EL & Philips SM (2010). Facts, noise and wishful thinking: muscle protein turnover in aging and human disuse atrophy. *Scand J Med Sci Sports* **20**, 5–9.

Saks V, Guzun R, Timohhina N, Tepp K, Varikmaa M, Monge C, Beraud N, Kaambre T, Kuznetsov A, Kadaja L, Eimre M & Seppet E (2010). Structure–function relationships in feedback regulation of energy fluxes in vivo in health and disease: mitochondrial interactosome. *Biochim Biophys Acta* **1797**, 678–697.

Saks VA, Belikova YO & Kuznetsov AV (1991). In vivo regulation of mitochondrial respiration in cardiomyocytes: specific restrictions for intracellular diffusion of ADP. *Biochim Biophys Acta* **1074**, 302–311.

Saks VA, Veksler VI, Kuznetsov AV, Kay L, Sikk P, Tiivel T, Tranqui L, Olivares J, Winkler K, Wiedemann F & Kunz WS (1998). Permeabilized cell and skinned fiber techniques in studies of mitochondrial function in vivo. *Mol Cell Biochem* **184**, 81–100.

Schiaffino S, Sandri M & Murgia M (2007). Activity-dependent signaling pathways controlling muscle diversity and plasticity. *Physiology (Bethesda)* **22**, 269–278.

Schwerzmann K, Hoppeler H, Kayar SR & Weibel ER (1989). Oxidative capacity of muscle and mitochondria: correlation of physiological, biochemical, and morphometric characteristics. *Proc Natl Acad Sci U S A* **86**, 1583–1587.

Sebastián D, Hernández-Alvarez MI, Segalés J, Sorianello E, Muñoz JP, Sala D, Waget A, Liesa M, Paz JC, Gopalacharyulu P, Orešič M, Pich S, Burcelin R, Palacín M & Zorzano A (2012). Mitofusin 2 (Mfn2) links mitochondrial and endoplasmic reticulum function with insulin signaling and is essential for normal glucose homeostasis. *Proc Natl Acad Sci U S A* **109**, 5523–5528.

Srere PA (1969). Citrate synthase. *Methods Enzymol* **13**, 3–11.

Svenson KL, Von Smith R, Magnani PA, Suetin HR, Paigen B, Naggert JK, Li R, Churchill GA & Peters LL (2007). Multiple trait measurements in 43 inbred mouse strains capture the phenotypic diversity characteristic of human populations. *J Appl Physiol* **102**, 2369–2378.

ter Veld F, Jeneson JA & Nicolay K (2005). Mitochondrial affinity for ADP is twofold lower in creatine kinase knock-out muscles. Possible role in rescuing cellular energy homeostasis. *FEBS J* **272**, 956–965.

Thomassen M, Rose AJ, Jensen TE, Maarbjerg SJ, Bune L, Leitges M, Richter EA, Bangsbo J & Nordsborg NB (2011). Protein kinase Cα activity is important for contraction-induced FXYD1 phosphorylation in skeletal muscle. *Am J Physiol Regul Integr Comp Physiol* **301**, R1808–R1814.

Tsintzas OK, Williams C, Boobis L & Greenhaff P (1995). Carbohydrate ingestion and glycogen utilization in different muscle fibre types in man. *J Physiol* **489**, 243–250.

Veksler VI, Kuznetsov AV, Sharov VG, Kapelko VI & Saks VA (1987). Mitochondrial respiratory parameters in cardiac tissue: a novel method of assessment by using saponin-skinned fibers. *Biochim Biophys Acta* **892**, 191–196.

Villani G, Greco M, Papa S & Attardi G (1998). Low reserve of cytochrome *c* oxidase capacity *in vivo* in the respiratory chain of a variety of human cell types. *J Biol Chem* **273**, 31829–31836.

Mouse Genome Sequencing Consortium, Waterston RH, Lindblad-Toh K, Birney E, Rogers J, Abril JF et al. (2002). Initial sequencing and comparative analysis of the mouse genome. Nature 420, 520-562. Consortium MGS, Waterston RH, Lindblad-Toh K, Birney E, Rogers J, Abril JF & al. e. (2002). Initial sequencing and comparative analysis of the mouse genome. *Nature* **420,** 520–562.

Yajid F, Mercier JG, Mercier BM, Dubouchaud H & Préfaut C (1998). Effects of 4 wk of hindlimb suspension on skeletal muscle mitochondrial respiration in rats. *J Appl Physiol* **84**, 479–485.

Supporting Information

Additional Supporting Information may be found in the online version of this article:

SUPPLEMENTAL FIGURE S1. Quantification of mitochondria-specific enzymes across mouse skeletal muscles. Using a subsection of animals (n = 4) the expression of various mitochondrial proteins were quantified (mean ± SD) in quadricep (QUAD, grey bars), soleus (SOL, black bars), and lateral gastrocnemius (GAST, white bars). The respective correlation of these values to citrate synthase (CS) activity was also examined in QUAD (grey filled points), SOL (black filled points), and GAST (white filled points). Protein quantification and correlation to CS activity for mitochondrial complex I (A & B), mitochondrial complex II (C&D), mitochondrial complex III (E & F), mitochondrial complex IV (G & H), mitochondrial complex V (I & J), 3-hydroxyacyl coenzyme a dehydrogenase (HAD, K & L), and CS (M & N).